Retina

Retinal Hemorheologic Characterization of Early-Stage Diabetic Retinopathy Using Adaptive Optics Scanning Laser Ophthalmoscopy

Shigeta Arichika, Akihito Uji, Tomoaki Murakami, Noriyuki Unoki, Shin Yoshitake, Yoko Dodo, Sotaro Ooto, Kazuaki Miyamoto, and Nagahisa Yoshimura

The Department of Ophthalmology and Visual Sciences, Kyoto University Graduate School of Medicine, Kyoto, Japan

PURPOSE. Adaptive optics scanning laser ophthalmoscopy (AO-SLO) is a noninvasive technique that allows for the direct monitoring of erythrocyte aggregates in retinal capillaries. We analyzed the retinal hemorheologic characteristics in normal subjects, diabetic patients without diabetic retinopathy (NDR), and diabetic patients with nonproliferative diabetic retinopathy (NPDR), using spatiotemporal (ST) blood flow images to visualize blood corpuscle trajectory.

METHODS. AO-SLO images of the parafoveal capillary network were acquired for three groups: 20 healthy volunteers, 17 diabetic patients with NDR (8 type 1 and 9 type 2 patients), and 10 diabetic patients with NPDR (4 type 1 and 6 type 2). The erythrocyte aggregate velocity assigned to a relative cardiac cycle and the elongation rate of the erythrocyte aggregate were calculated.

RESULTS. Careful observation revealed that flow velocity fluctuations were found with higher frequency in diabetic patients than in normal subjects. The total average velocities were 1.26 $\pm$ 0.22 mm/s in the normal group, 1.31 $\pm$ 0.21 mm/s in the NDR group, and 1.63 $\pm$ 0.35 mm/s in the NPDR group. The average velocities of the NPDR group were higher than those in the normal ($P = 0.001$) and NDR ($P = 0.009$) groups. The average elongation rates of the 3 groups were 0.67 $\pm$ 0.20, 0.39 $\pm$ 0.19, and 0.33 $\pm$ 0.11, respectively. Elongation rate differed significantly between the normal and NDR ($P = 0.003$) groups as well as the normal and NPDR ($P = 0.001$) groups.

CONCLUSIONS. AO-SLO can be used to detect retinal hemorheologic changes in the early stages of diabetic retinopathy.

Keywords: diabetic retinopathy, AO-SLO, hemorheology

Diabetic retinopathy (DR) is a leading cause of blindness.[1,2] Because the early detection of DR is important in the prevention of DR progression[3,4] as well as cardiovascular events[5–7] and stroke,[7] effective tools with which to screen for DR are needed. Fundus examinations by ophthalmoscopy and color fundus photography have long been considered the gold standards for diagnosing and staging DR. Although imaging technology in the field of ophthalmology, including optical coherence tomography (OCT), has advanced rapidly in recent decades, no other useful method for the diagnosis of DR has been established for the detection of signs that appear earlier than the microaneurysm (MA), the earliest clinical sign[8] detectable by routine fundus examination. The ability to detect microlesions secondary to DR before the manifestation of clinically apparent retinopathy would improve the patient's visual prognosis and quality of life.

The pathogenesis of DR is characterized by histopathologic changes, such as a loss of pericytes,[9] endothelial cell death,[9,10] thickening of the basement membrane,[9] and leukocyte adherence to the retinal vascular endothelium,[10] as well as hemorheologic changes, such as reduced leukocyte deformability,[11] reduced erythrocyte deformability,[12,13] increased erythrocyte aggregation,[12,14,15] and increased platelet aggrega-

tion.[16] In order to analyze abnormal hemodynamics with the potential to elucidate pathologic changes other than clinically detectable morphological changes in DR, retinal blood flow measurements were obtained using various techniques and at various stages of type 1 and type 2 DR. The technologies presented here will facilitate research on DR as well as other types of retina pathophysiology.[17,18] Their development is therefore believed to be capable of catalyzing dramatic breakthroughs in the development of tools for the early diagnosis of retinal disorders.

Erythrocytes play an important role in the hemorheology of vascular disease.[12,13,19] Erythrocyte aggregation is considered to be an important hemorheologic parameter in DR because the increase in erythrocyte aggregation[12–14] prevents erythrocytes from passing through the capillaries.[13] Further investigations of retinal hemodynamics at the level of the capillary are needed. To date, the gold standard for evaluating human retinal capillaries has been fluorescein angiography, which carries a risk of allergic reaction.

Adaptive optics scanning laser ophthalmoscopy (AO-SLO) is a promising technology that can be used to image the retinal microvasculature noninvasively, objectively, and directly (Fig. 1).[20–28] Adaptive optics allows the researcher to correct for
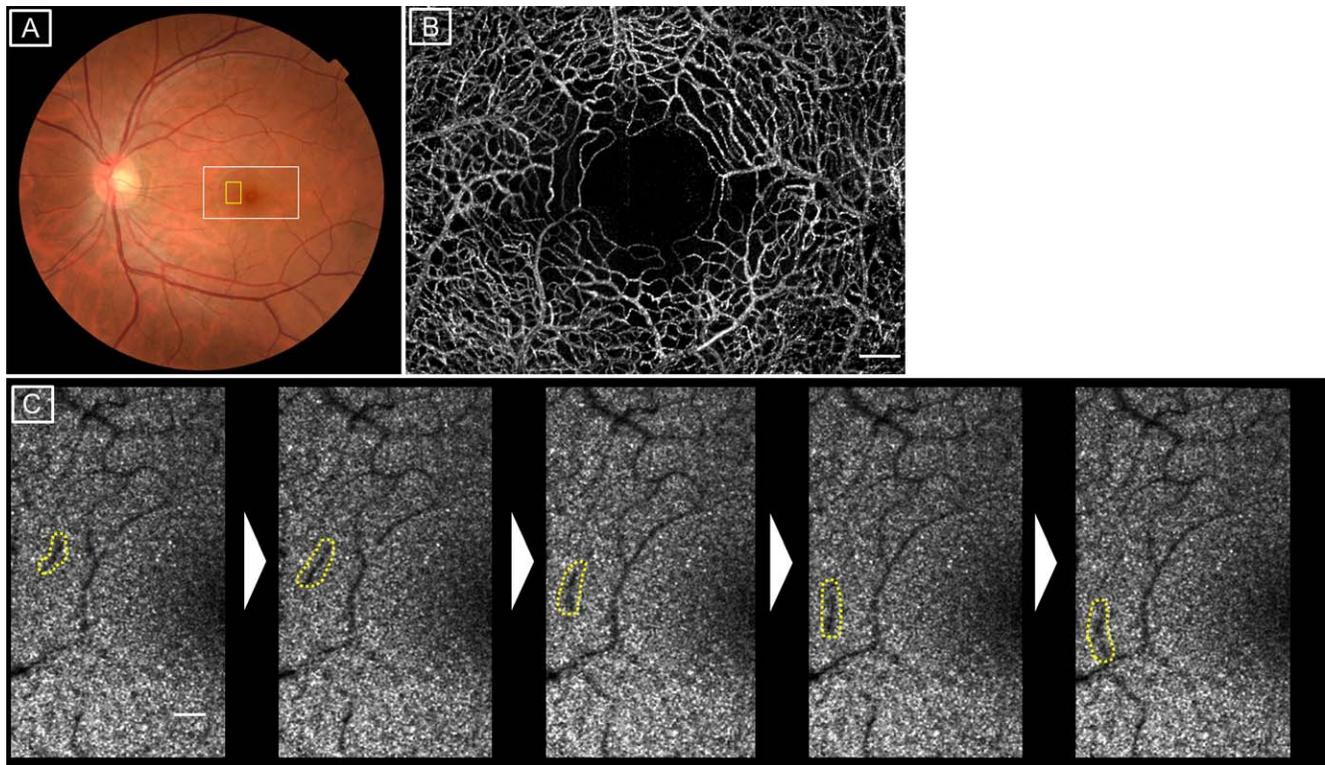
FIGURE 1. Microcirculation network information detected by AO-SLO. (**A**) Fundus photograph of the left eye in a normal subject. (**B**) Montage of the foveal microvasculature (perfusion map) obtained noninvasively by using the motion contrast-enhancement technique from AO-SLO images without any dying agents. The montage corresponds to the *white* outlined area in the fundus photograph (**A**). *Scale bar*: 200 µm. (**C**) Five consecutive frames acquired by AO-SLO correspond to the area outlined in *yellow* in the fundus photograph (**A**) showing the moving erythrocyte aggregates (*yellow dotted line*). AO-SLO imaging was performed by focusing on the photoreceptor layer to detect the cone mosaic pattern. Numerous bright dots represent cones. Capillaries appear as dark shadows on the bright cone mosaic. The example shown in (**C**) depicts the area of sampling used in this study. *Scale bar*: 100 µm.

ocular aberrations and provides high-resolution retinal images that capture photoreceptors,[20] blood flow,[21,22,28] blood corpuscles,[23,24] capillary networks,[25] retinal wall,[26] and the retinal nerve fiber layer.[27] Considering that early retinal diabetic changes originate from microcirculatory disturbances,[29] AO-SLO, which can be used to observe blood corpuscles in the parafovea directly, could be used to evaluate retinal hemorheology in capillary networks. Herein, we analyzed the characteristics of erythrocyte aggregate movement in parafoveal capillary networks of patients with early-stage DR, directly and noninvasively, using AO-SLO.

METHODS

This study was approved by the Institutional Review Board and the Ethics Committee at Kyoto University Graduate School of Medicine. All aspects of study conduct adhered to the tenets of the Declaration of Helsinki. Written informed consent was obtained from each participant after the nature of the study and the risks and benefits of study participation were thoroughly explained.

Subjects

Adaptive optics scanning laser ophthalmoscopy movies were acquired for 20 healthy Japanese volunteers (mean age ± standard deviation, 36.7 ± 11.5 years; range, 20–61 years); 17 diabetic patients without DR (NDR) (8 type 1 and 9 type 2 patients; 39.9 ± 11.7 years; range, 20–55 years); and 10

diabetic patients with nonproliferative DR (NPDR) (4 type 1 and 6 type 2 patients; 39.9 ± 13.6 years; range, 22–59 years). Diabetes type was determined from internal medical records. The international clinical classification was determined by retinal specialists through indirect ophthalmoscopic fundus examination and slit lamp biomicroscopic fundus. A fundus photograph was obtained for all patients.[30] The exclusion criteria were as follows: contraindication to pupil dilation, best-corrected visual acuity worse than 20/25, refractive error > 5.0 or < −6.0 diopters, axial length > 26 mm, intraocular pressure > 21 mm Hg, macular edema, bilateral difference on the stage of DR, prior ocular surgery, hypertension, secondary DM, and pregnancy. All subjects were dilated before AO-SLO image acquisition with 1 drop of tropicamide (0.5%) and phenylephrine hydrochloride (0.5%). Following pupil dilation, subjects were examined for approximately 20 minutes in total per eye while they remained in a seated posture.

Adaptive Optics Scanning Laser Ophthalmoscopy Imaging

The AO-SLO system developed by Canon (Canon, Inc., Tokyo, Japan)[23,24,31] is composed of the AO system, a high-resolution confocal SLO imaging system, and a wide-field imaging subsystem. The imaging wavelength was 840 ± 25 nm, and the wavelength of beacon light for the measurement of wave front aberrations was 760 ± 5 nm. The imaging light and the beacon light were set at 330 and 40 µW, respectively, by calculating the incident power of both light sources in

accordance with the safety limits set by the American National Standards Institute.[32] Multiple high-resolution retinal videos were acquired from the eyes until the entire parafoveal area had been imaged. Videos were recorded for 2 to 4 seconds per scan area, with a field size of $1.4 \times 2.8°$, and were collected for each subject to cover the parafoveal areas. AO-SLO videos from the temporal and nasal areas located 0.25 to 0.5 mm from the foveal center were chosen for analysis, and all observed erythrocyte aggregates were used for analysis. All erythrocyte aggregate velocities were analyzed on movies recorded at a rate of 64 frames/s. All AO-SLO imaging was performed with the optical focus on the photoreceptor layer.[23,24] All target vessels were free of bifurcations within the imaged area. As reported previously,[33] axial length measurements were obtained using an optical biometer (IOL Master; Carl Zeiss Meditec, Dublin, CA, USA). The AO-SLO image angle was converted to the actual distance to the retina based on each subject's measured axial length using the AO-SLO Retinal Image Analyzer (ARIA; Canon, Inc.) software dedicated to our prototype AO-SLO. Adaptive optics imaging and ocular grading were conducted on the same day, in the morning.

Blood Component Discrimination in Adaptive Optics Scanning Laser Ophthalmoscopy Videos

The transparency of leukocytes to the AO-SLO laser enables leukocytes to be identified as bright, moving objects, which represent light reflected from the photoreceptors within the optical focus of the photoreceptor layer. The AO-SLO laser does not pass through erythrocyte aggregates, which are depicted as black moving objects.[23] Blood components were identified using spatiotemporal (ST) images, according to the methods proposed by our previous report.[28] Briefly, leukocyte traces were identified as follows: thick, high contrast, sparse, and unidirectional. Plasma gap traces, which tended to have lower contrast than leukocyte traces, were identified as thin and dense. Erythrocyte aggregate traces following leukocyte traces were identified as thick, high contrast, and hyporeflective.[24]

Evaluation of the Rheological Properties of Erythrocyte Aggregates

Velocity Measurement. We investigated the aggregated erythrocytes that blocked the AO-SLO laser, creating shadows. Erythrocyte aggregates were described as dark regions (darker than the vessel shadow) that occurred closely behind leukocytes (Supplementary Movie S1). Considering that the erythrocyte aggregates followed the leukocytes, the velocity for the head of the erythrocyte aggregate was equivalent to the velocity of the leukocyte's tail end. The method used to measure velocity has previously been described in full.[24] Briefly, ST images for AO-SLO movies on the target vessels, which were free from bifurcations, showed a white band and black band corresponding primarily to the trajectories of moving leukocytes and erythrocyte aggregates, respectively (Fig. 2). The head end of erythrocyte aggregate velocities, which was equivalent to the tail end of leukocyte velocities on ST images, was obtained by calculating the reciprocal of the slope of the borderline between the white and black bands depicted in the ST image. In order to synchronize velocity and cardiac pulsation, a pulse oximeter (Oxypal Neo; Nihon Kohden, Tokyo, Japan) was attached to the subject's earlobe. Referring to the Martin et al.[22] report, the measurements were divided into five equal bins, each corresponding to the segment of the cardiac cycle in which they were observed to correct for the influence of cardiac pulsation on measured velocities (Fig. 3). The overall average velocity of all five bins was then calculated by averaging the mean velocities of

individual bins. The pulsatility index (PI) was calculated as follows, according to the methods proposed by Tam et al.[34]

$$PI = \frac{V\max - V\min}{V\mean} \quad (1)$$

where PI, V_{max}, V_{min}, and V_{mean} represent pulsatility index, the maximum velocity of individual bins, the minimum velocity of individual bins, and the overall average velocity of individual bins, respectively. The velocities for microaneurysm and tortuosity in NPDR group are not included for analysis to exclude the direct influence of turbulent flow.

Erythrocyte Aggregate Elongation Rate Analysis. The elongation of erythrocyte aggregates in a time-dependent manner in the parafoveal capillaries is a normal finding that can be observed in healthy subjects.[24] In the current study, the elongation rate of erythrocyte aggregates was calculated by means of ST images, as described in our previous paper (Fig. 4).[24]

Reproducibility of the Measurement of Velocity and Erythrocyte Aggregate Elongation Rate. In order to evaluate the reproducibility of the measurement of velocity and erythrocyte aggregate elongation rate, the same vessels in five normal subjects were analyzed on 3 different days within a period of 2 months.

Categorization of Spatiotemporal Images. The characteristics of ST images were compared among the groups to analyze the associated rheological properties. Further observation of ST images for the vessel containing the erythrocyte aggregates made it possible to categorize the ST images into four groups (Fig. 2). The patterns were categorized into the following types: (1) white and black bands that gradually widened, (2) white and black bands that started wider than type 1 bands and then increased in width, (3) both bands exhibited minor changes in width, (4) band slope bent concavely or convexly while traveling through a vessel free of bifurcations, which meant that the velocities changed in a time-dependent fashion. The ST images were categorized by two ophthalmologists after visual inspection. The assessment was performed with the assessors blinded to participant information. When the categorization differed among the assessors, the type was determined based on a discussion with reference to the AO-SLO movies.

Statistical Analyses

All values are presented as mean ± standard deviation. Comparisons of the ages, average velocities of erythrocyte aggregates, maximum velocities of individual bins, minimum velocities of individual bins, elongation rate of erythrocyte aggregates, and pulsatility index among the groups were carried out using 1-way ANOVA, with post hoc comparisons tested using the Scheffe test. The difference in the characteristics between patients without diabetic retinopathy and those with nonproliferative diabetic retinopathy as well as the difference in the HbA1c levels between the NDR and NPDR groups were analyzed using a Mann-Whitney U test. The relationships between the erythrocyte aggregate velocities and HbA1c and between erythrocyte aggregate elongation rate and HbA1c were analyzed using the Pearson correlation coefficient. The velocity and erythrocyte aggregate elongation rate measurements performed on three different days were compared using repeated-measures ANOVA. Comparisons of velocities over the pulse cycle among the normal group, NDR group, and NPDR group were carried out using repeated-measures ANOVA. All analyses were performed using StatView (Version 5.0; SAS Institute, Cary, NC, USA). A P value < 0.05 was considered statistically significant.
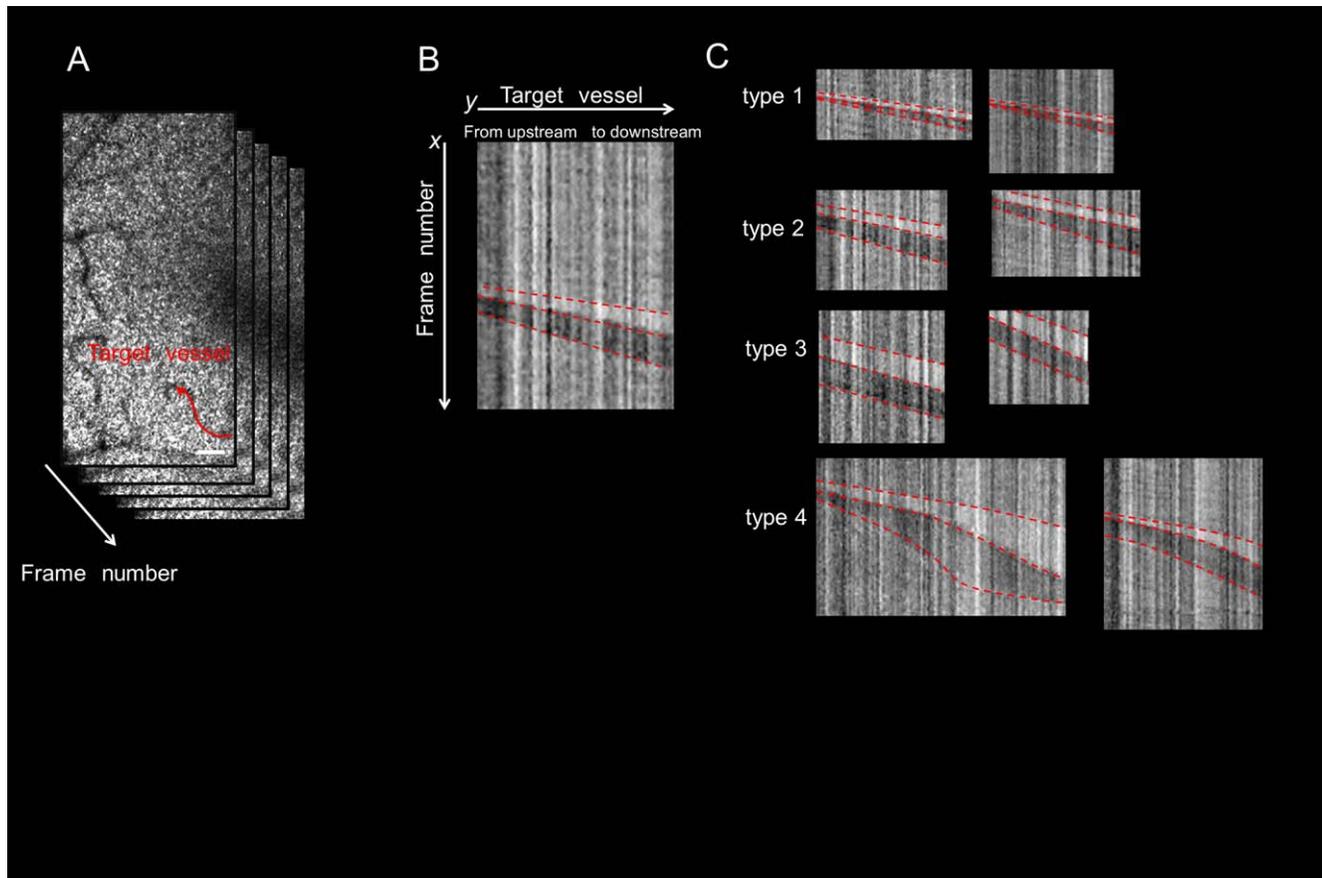
Figure 2. The characterization of STl images generated from AO-SLO videos of the parafoveal capillary network. (**A**) The target vessel on the consecutive frames of the AO-SLO. The *red line* represents the target vessel for analysis. *Scale bar*: 100 μm. (**B**) The ST image generated from the AO-SLO video by reslicing the frames along the line set on the target vessel. The white band paired with dark bands correspond to the trajectories of leukocytes (mainly) and erythrocyte aggregates, respectively. The *topmost red dashed line* represents the head of the white band. The *middle red dashed line* represents the border between the white and black bands, and the inverse of this slope corresponds to the head of erythrocyte aggregate velocity. The *bottommost red dashed line* represents the tail end of the black band. (**C**) The categorization of ST images into four types include the following: type 1, white and black bands widen gradually; type 2, white and black bands start out wider than type 1, then widen; type 3, both bands exhibit small changes in width; type 4, the slope of the bands bends concavely or convexly when traveling in a vessel free of bifurcations.

RESULTS

The characteristics of diabetic patients are listed in the Table. No significant difference was found in age among the groups ($P = 0.67$). The average axial lengths were 24.8 ± 1.2 mm in the normal group, 24.4 ± 0.9 mm in the NDR group, and 24.2 ± 1.1 mm in the NPDR group, with no significant difference among the groups ($P = 0.36$). The average HbA1c level was 9.1 ± 1.9 in the NDR group and 8.7 ± 1.8 in the NPDR group, with no significant difference between groups ($P = 0.95$).

Reproducibility of the Measurement of Velocity and Erythrocyte Aggregate Elongation Rate

The overall average velocities of five bins in five normal subjects were 1.25 ± 0.36 mm/s during the first measurement, 1.24 ± 0.38 mm/s during the second, and 1.34 ± 0.45 mm/s during the third ($P = 0.27$) (Supplementary Fig. S1). The total average erythrocyte elongation rate in five normal subjects was 0.85 ± 0.23 during the first measurement, 0.74 ± 0.12 during the second, and 0.94 ± 0.19 during the third ($P = 0.18$) (Supplementary Fig. S1). No significant difference was observed among the three velocity and erythrocyte aggregate elongation rate measurements.

Rapid Changes in Erythrocyte Aggregate Velocities in Diabetic Patients

In total, images of sufficient quality for the calculation of velocity were obtained for 768 erythrocyte aggregates from 20 (100%) normal subjects, 500 erythrocyte aggregates from 17 (100%) patients with NDR, and 173 erythrocyte aggregates from 10 (100%) patients with NPDR. Although all velocity calculations were performed relative to the cardiac cycle at average velocity, interestingly, one vessel with two erythrocyte aggregates from one (5.0%) normal subject, six vessels with nine erythrocyte aggregates from five (29.4%) patients with NDR, and six vessels with nine erythrocyte aggregates from five (50.0%) patients with NPDR showed rapid velocity changes in type 4 ST images, showing the bands bent concavely or convexly while traveling through a vessel free of bifurcations (Fig. 2; Supplementary Movie S2). These inconstant velocities were excluded from the analyses of average velocity, PI, and elongation rate.

Differences in Erythrocyte Aggregate Velocity Between Normal Subjects and Diabetic Patients

In the normal group, the overall average velocity of all five bins was 1.26 ± 0.22 mm/s; average velocities of individual bins
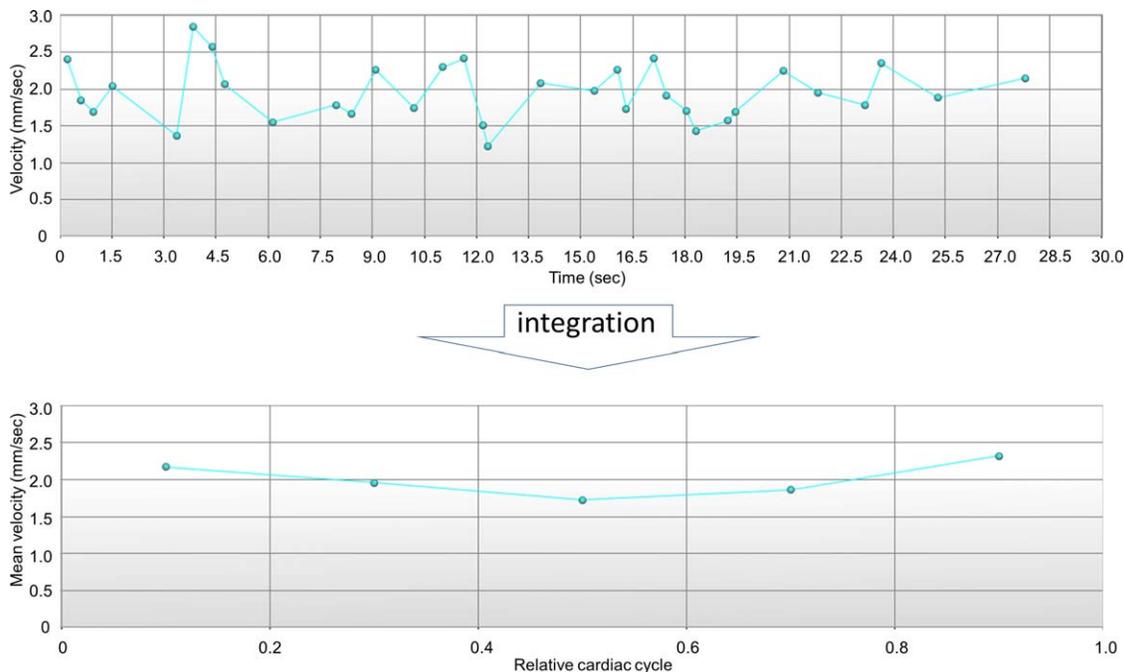
FIGURE 3. Velocity and cardiac pulsation synchronization. The sphygmogram was digitized and recorded during the imaging session. The AO-SLO image analysis software detected extreme values from the sphygmogram and then determined the relative cardiac cycle for each frame of the captured AO-SLO video. By dividing the relative cardiac cycle into 5 equal segments and averaging the raw velocities within each segment, mean erythrocyte aggregate velocity was plotted against relative cardiac cycle.
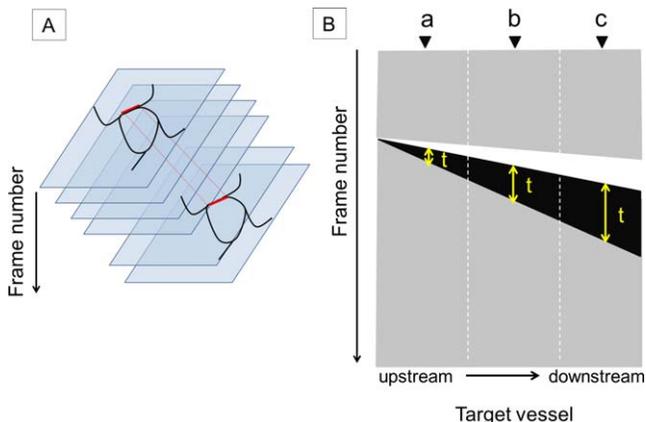

FIGURE 4. Measurement of erythrocyte aggregate velocity and length using spatiotemporal images. (A) Stacked sequential frames of the AO-SLO video. Frames are resliced along the *red line* set on the target vessel in order to generate the ST image. (B) Erythrocyte aggregate velocity and length were calculated using the ST image plotted with the length of the target vessel on the horizontal axis and the frame number on the vertical axis. The *white band* and the wider *black band* represent the trajectory of moving leukocytes (mostly) and erythrocyte aggregates, respectively. The thickness of the *black band* (t) represents the time required for the dark tail to pass through a point located on the target vessel. The reciprocal of the slope of the border between the *white* and *black bands* represents the velocity of the head of the erythrocyte aggregate. The ST image was vertically separated into three zones from upstream to downstream with respect to blood flow (zones a, b, and c). Erythrocyte aggregate length was calculated by multiplying the velocity by the time required to evaluate the elongation rate for each zone.

TABLE. Characteristics of Diabetic Patients

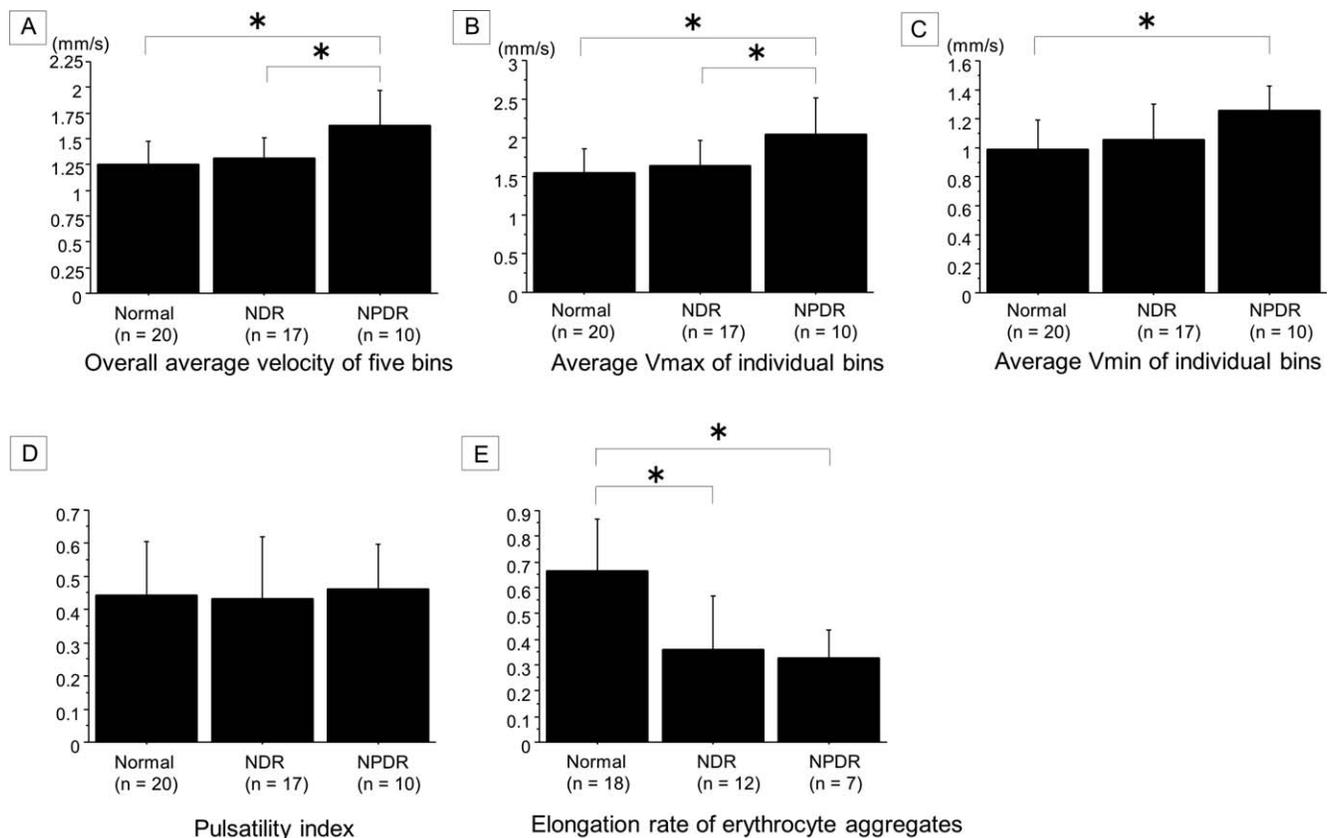|	Patients Without Diabetic Retinopathy	Patients With Nonproliferative Diabetic Retinopathy	P Value
Age, y	39.9 ± 11.7	39.9 ± 13.6	0.997
Sex (male/female)	9/8	6/4	
Diabetic type (type1/type2)	8/9	4/6	–
Stage of nonproliferative diabetic retinopathy			
Mild	NA	5	
Moderate	NA	5	
Severe	NA	0	–
HbA1c, %	9.1 ± 1.8	8.7 ± 1.8	0.606
Duration of diabetes, y	3.69 ± 3.47	14.8 ± 6.8	<0.0001
Medications			
Diet	1	0	
Insulin	11	4	
Oral	4	1	
Insulin and oral	1	5	–
Blood pressure, mm Hg			
Systolic	114 ± 15	124 ± 10	0.104
Diastolic	71 ± 14	77 ± 12	0.302
Intraocular pressure, mm Hg	14.2 ± 2.7	15.7 ± 2.6	0.179
Red blood cells, ×10⁴/mm³	479 ± 44	492 ± 47	0.477
White blood cells, mm³	6982 ± 2293	5699 ± 922	0.105

NA indicates not applicable.

FIGURE 5. Comparison of erythrocyte aggregate velocity, elongation rate, and pulsatility index among normal subjects, patients without diabetic retinopathy, and patients with NPDR. (**A**) The overall averaged velocity for the 5 bins in the NPDR group was significantly higher than that of the normal group ($P = 0.001$) and the group without diabetic retinopathy (NDR) ($P = 0.009$). There were no significant differences between the normal group and the NDR group in overall average velocities. (**B**) The maximum velocities of individual bins in the NPDR group were significantly higher than those in the normal group ($P = 0.003$) and the NDR group ($P = 0.02$). Significant difference was not observed between the normal group and the NDR group. (**C**) The minimum velocities of individual bins in the NPDR group were significantly higher than those in the normal group ($P = 0.007$). No significant differences were observed between the normal group and the NDR group or between the NDR group and the NPDR group. (**D**) No significant differences in PI were detected among the groups. (**E**) Elongation rates in the NDR group ($P = 0.003$) and NPDR ($P = 0.001$) group were significantly lower than those in the normal group; however, there was no difference in elongation rate between the NDR group and the NPDR group ($P = 0.93$). V_{max} indicates maximum velocity; V_{min}, minimum velocity. *$P < 0.05$, 1-way ANOVA, with post hoc comparisons tested using the Scheffe test.

ranged from 1.04 to 1.45 mm/s, and individual erythrocyte aggregate velocities measured for all subjects ranged from 0.36 to 3.43 mm/s. In the NDR group, the overall average velocity of all five bins was 1.31 ± 0.21 mm/s; average velocities of individual bins ranged from 1.21 to 1.45 mm/s, and individual erythrocyte aggregate velocities measured for all subjects ranged from 0.46 to 4.01 mm/s. In the NPDR group, the overall average velocity of all five bins was 1.63 ± 0.35 mm/s; average velocities of individual bins ranged from 1.44 to 1.87 mm/s, and individual erythrocyte aggregate velocities measured for all subjects ranged from 0.71 to 4.19 mm/s (Supplementary Movie S3). There were no significant differences between the normal group and the NDR group in overall average velocity ($P = 0.789$) (Fig. 5A). The overall velocities in the NPDR group were significantly higher than those in the normal group ($P = 0.001$) and those in the NDR group ($P = 0.009$). The maximum velocities of individual bins in the NPDR group were significantly higher than those in the normal group ($P = 0.003$) and the NDR group ($P = 0.02$) (Fig. 5B). Significant difference was not observed between the normal group and the NDR group ($P = 0.77$). The minimum velocities of individual bins in the NPDR group were significantly higher than those in the normal group ($P = 0.007$) (Fig. 5C). No

significant differences were observed between the normal group and the NDR group ($P = 0.585$) or between the NDR group and the NPDR group ($P = 0.07$). Periodic shifts of velocity related to pulsation were observed in three groups (Fig. 6). Tendencies toward higher velocity during diastole and a lower velocity during systole were observed in all three groups ($P < 0.001$ for the normal group; $P = 0.003$, NDR group; and $P = 0.01$, NPDR group). The average PI was 0.44 ± 0.16 in the normal group, 0.43 ± 0.19 in the NDR group, and 0.46 ± 0.13 in the NPDR group. No significant differences in PI were detected among the groups ($P = 0.89$) (Fig. 5D).

Differences in the Erythrocyte Aggregate Elongation Rate

The elongation rates of 66 erythrocyte aggregates from 18 (90.0%) of 20 normal subjects, 45 erythrocyte aggregates from 12 (70.6%) of 17 patients with NDR, and 19 erythrocyte aggregates from 7 (70.0%) of 10 patients with NPDR were calculated successfully. The remaining subjects were excluded from the analysis of erythrocyte aggregate elongation because of the poor quality of the ST images. In these images, the bottom line of the erythrocyte aggregate corresponded to the
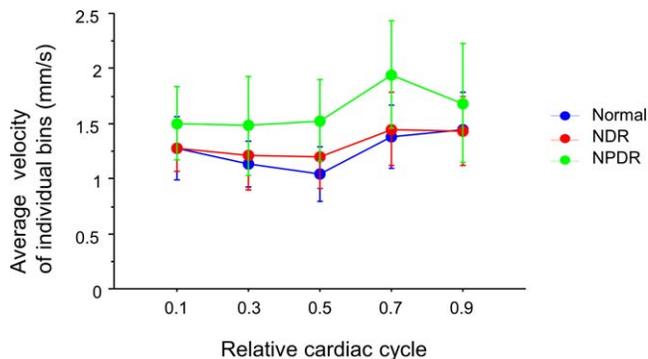
FIGURE 6. Pulsation of blood flow as detected in normal subjects, patients with NDR, and patients with NPDR. A relative cardiac cycle was assigned to each erythrocyte aggregate velocity in order to investigate the effect of cardiac pulsation on velocity. Velocity fluctuation was detected in a single relative cardiac cycle for all three groups. The maximum velocities tended to be observed in bins assigned to 0.7 or 0.9, which corresponded roughly to the diastolic phase. Meanwhile, minimum velocities were observed in the bin assigned to 0.5, which corresponded to the systolic phase. Statistical significances were found in the normal group ($P < 0.001$), in the NDR group ($P = 0.003$), and in the NPDR group ($P = 0.01$). The average pulsatility index values were 0.44 ± 0.16 in the normal group, 0.43 ± 0.19 in the NDR group, and 0.46 ± 0.13 in the NPDR group.

trajectory of the tail end of the erythrocyte aggregate and was not depicted clearly. The average elongation rates were 0.67 ± 0.20 in the normal group, 0.39 ± 0.19 in the NDR group, and 0.33 ± 0.11 in the NPDR group, respectively. Elongation rates in the NDR group ($P = 0.003$) and NPDR group ($P = 0.001$) were significantly lower than those in the normal group (Fig. 5E). However, there was no difference in elongation rate between the NDR group and the NPDR group ($P = 0.93$).

Categorization of Spatiotemporal Images

In total, 71 ST images from 18 (90%) normal subjects, 56 from 14 (82.4%) patients with NDR, and 36 from 7 (70.0%) patients with NPDR were used to categorize ST image type. The percentage of each type was as follows: 38.0% for type 1, 52.1% for type 2, 7.0% for type 3, and 2.8% for type 4 in the normal group; 16.1% for type 1, 42.9% for type 2, 25.0% for type 3, and 16.1% for type 4 in the NDR group; 13.9% for type 1, 30.6% for type 2, 30.6% for type 3, and 25.0% for type 4 in the NPDR group (Fig. 7). The NDR group and NPDR group had lower proportions of type 1 and type 2 and higher proportions of types 3 and 4 compared with the normal group.

Correlations Among Erythrocyte Aggregate Velocity, Elongation Rate, and HbA1c Level

In the NDR group, velocity had a tendency to correlate negatively with HbA1c levels, but the trend was not significant ($P = 0.09$, $r = -0.44$). No correlation was found between velocities and HbA1c levels in the NPDR group ($P = 0.73$, $r = 0.13$). A significant correlation was observed between the elongation rate and HbA1c negativity in the NDR group ($P = 0.002$, $r = -0.76$) and positivity in the NPDR group ($P = 0.02$, $r = 0.81$).

DISCUSSION

The aim of this study was to investigate hemorheologic properties in diabetic patients using AO-SLO, which allows for the direct and noninvasive visualization of retinal hemorheology in diabetic patients. Careful observation of the AO videos revealed that flow velocity fluctuations were found with higher frequency in diabetic patients than in normal subjects, suggesting that the hemorheologic changes in diabetic patients are captured accurately by AO videos. Although differences in erythrocyte aggregate velocity in the parafoveal network were found between normal subjects and NPDR patients, but not between normal subjects and NDR patients, erythrocyte aggregates in NDR patients who have no clinical appearance of retinopathy and NPDR patients showed lower elongation rates than those observed in normal subjects. Moreover, ST images that showed time-dependent changes in blood corpuscle arrangements and deformations could be categorized into four types. Differences in the proportion of each type of ST image were found between normal subjects and diabetic patients, suggesting that ST images can be used to visualize subclinical rheologic changes related to retinopathy in diabetic patients.

Retinal blood flow velocity changes associated with DM have long been investigated. In particular, the ability to measure velocity in NDR or early-stage DR has important implications for the early detection of retinopathy. However, the challenges inherent in these measurements have resulted in conflicting reports.[34,35] Considering only the results from research on human capillaries, it seems that blood flow velocity is decreased in diabetic patients.[34] To our knowledge, Tam et al.[34] published the first and only report on blood flow velocity in the retinal capillaries of diabetic patients as measured using AO-SLO. Their results showed that the velocities in seven type 2 diabetic patients with NDR were 14% lower than those of eight nondiabetic controls, but the trend lacked statistical significance. However, in this study, there was no significant difference in the overall average velocity of erythrocyte aggregates in the parafoveal capillary network between patients with NDR and nondiabetic controls, although retinal blood flow changes were reported as a primary reflection of retinal vascular endothelial dysfunction resulting from diabetes-related metabolic abnormalities.[36] One of the possible reasons for this difference in velocity could be the presence or absence of vessels with flow velocity fluctuations, which could lead to the measurement of extremely slow flow velocities. Because we excluded these vessels—which might represent leukostasis—from the analysis because of the difficulty in calculating accurate mean velocities, our results may have overestimated velocity in diabetic patients, as compared with other studies. Another potential reason for the discrepancy is that diabetic control statuses differ from study to study because retinal blood flow is modulated by glycemic control. Lorenzi et al.[37] reported that type 1 diabetic patients with no or minimal retinopathy who maintain relatively good glycemic control did not show abnormalities of the arterial retinal circulation as measured using laser Doppler flowmetry. Clermont and Bursell reported that there was a significant negative association between retinal blood flow and glycemic control.[36] Actually, in this study, the overall average velocities tended to correlate negatively with HbA1c levels in the NDR group; therefore, the distribution of diabetic control status may have affected our measurements of velocity in patients with NDR.

Calculating the velocity of moving objects in sequential video frames using ST images is a popular digital image–processing technique in the field of biomedical research.[38,39] In this study, we used ST images generated from capillary blood flow to map not only velocity but also the arrangements and deformations of blood corpuscles, which enabled us to visually understand the hemorheologic conditions in a given eye. The results showed differences in the types of ST images obtained
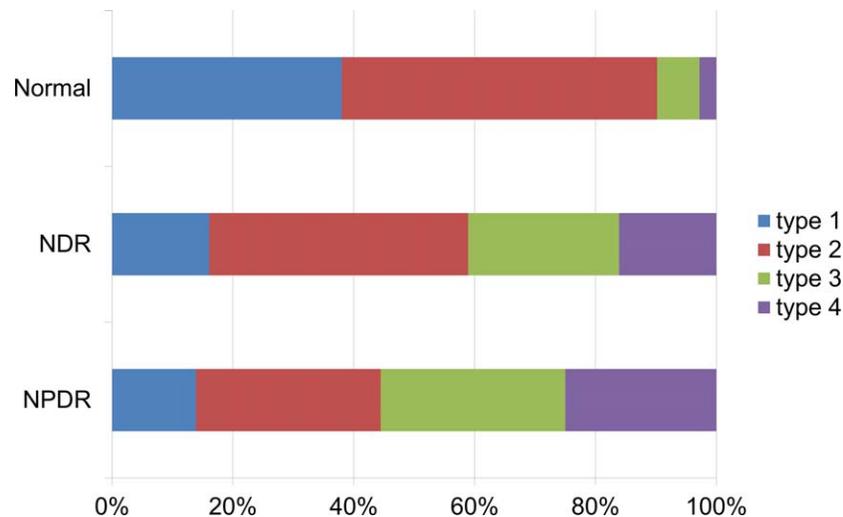
FIGURE 7. Histogram representing the ratio of ST image types in normal subjects, patients with NDR, and patients with NPDR. The NDR and NPDR groups had lower proportions of types 1 and 2 and much higher proportions of type 3 images, which represented minor changes in the elongation rate of erythrocyte aggregates, and type 4, which represented the presence of velocity changes in comparison with the normal group.

between normal subjects and diabetic patients. Type 1 and type 2 images, which represent the gradual elongation of erythrocyte aggregates, were more common in normal subjects, while type 3 images, which represented minor changes in elongation, and type 4, which represented flow velocity fluctuation, were seen only rarely. In contrast, diabetic patients had fewer type 1 and 2 images and more type 3 and 4 images when compared with normal subjects. Notably, types 3 and 4 accounted for more than 50% of the ST images obtained for NPDR patients. For further investigation, characteristics of the ST images, with the exception of type 4 ST images, were quantified by calculating the rate of erythrocyte aggregate elongation. Subsequent analyses verified that elongation rate was significantly lower in patients with NDR and NPDR as compared to normal subjects, and the erythrocyte aggregate elongation rates and HbA1c levels correlated significantly and negatively in the NDR group, suggesting that hemorheologic changes are apparent in AO-SLO videos before the clinical appearance of DR. Notably, one factor that can decrease the elongation rate of erythrocyte aggregates is the reduced deformability of erythrocytes in DM patients. Although erythrocytes can deform to pass through capillaries, the deformability of erythrocytes in patients with DM is reduced.[12,13] The reduced deformability of erythrocytes can prevent the cell from entering the capillary and consequently decrease the elongation rate in the microcirculation. Increased erythrocyte aggregability can also decrease the elongation rate in DM, perhaps by promoting the production of erythrocyte aggregates and the elongation of erythrocyte aggregates.[13] Taking into consideration that the total count of erythrocytes is limited, reduced numbers of isolated erythrocytes could also lead to a decrease in the elongation rate.

Significant changes in velocity and elongation rate were noted at different stages of DR. These results led us to speculate that vessel morphology might contribute to velocity changes, as changes in velocity occur after the clinical appearance of DR. The reduced elongation rate of erythrocyte aggregates could be considered to be a result of changes in deformability and aggregability. One potential reason for the differences in velocity between NDR and NPDR may be that leukocytes and erythrocyte aggregates have preferred pathways,[28,40] while neither cell type tends to pass through plasma gap capillaries (PGCs). As Tam et al.[21] theorized that leukocyte

preferred paths (LPPs) might prevent leukocytes from entering non-LPP capillaries and PGCs may serve as relief valves to minimize flow disruption when a leukocyte enters a nearby LPP, PGCs may work to curb the increase in blood cell velocity in LPPs or erythrocyte aggregate preferred paths in NDR. Impaired flow through PGCs may increase the velocity of blood cells in nearby LPPs. Nonetheless, the impairment of LPPs or erythrocyte aggregate preferred pathways may force leukocytes or erythrocyte aggregates to enter PGCs, which may lead to intravascular stasis, in a vicious circle.

One limitation of this study was the relatively small sample size. Although significant correlation was observed between the elongation rate and HbA1c negativity in the NDR group and positivity in the NPDR group, it was difficult to interpret the reverse correlation. To achieve this, an appropriate sample size is required. An increase in the rate of successful image acquisition could be achieved by further developing the associated hardware and software, which in turn could enable larger studies in the future. Another limitation of this study is the lack of a longitudinal study, which is required to determine which patients will progress and which predictive value can be considered.

In conclusion, AO-SLO movies represent a noninvasive tool that provides hemorheologic information that can be used to measure the velocity and elongation rate of erythrocyte aggregates in patients with DM. Optics scanning laser ophthalmoscopy technology could shed light on investigations of the microcirculation in diabetic patients.

Disclosure: **S. Arichika**, None; **A. Uji**, None; **T. Murakami**, None; **N. Unoki**, None; **S. Yoshitake**, None; **Y. Dodo**, None; **S. Ooto**, None; **K. Miyamoto**, None; **N. Yoshimura**, Topcon Corporation (F), Nidek (F, C), Canon (F)

References

1. Yau JW, Rogers SL, Kawasaki R, et al. Global prevalence and major risk factors of diabetic retinopathy. *Diabetes Care*. 2012; 35:556–564.

2. Kempen JH, O'Colmain BJ, Leske MC, et al. The prevalence of diabetic retinopathy among adults in the United States. *Arch Ophthalmol*. 2004;122:552–563.

3. The effect of intensive treatment of diabetes on the development and progression of long-term complications in insulin-dependent diabetes mellitus. The Diabetes Control and Complications Trial Research Group. *N Engl J Med*. 1993;329: 977–986.

4. Shichiri M, Kishikawa H, Ohkubo Y, Wake N. Long-term results of the Kumamoto Study on optimal diabetes control in type 2 diabetic patients. *Diabetes Care*. 2000;23(suppl 2):B21–29.

5. Kramer CK, Rodrigues TC, Canani LH, Gross JL, Azevedo MJ. Diabetic retinopathy predicts all-cause mortality and cardiovascular events in both type 1 and 2 diabetes: meta-analysis of observational studies. *Diabetes Care*. 2011;34:1238–1244.

6. Juutilainen A, Lehto S, Ronnemaa T, Pyorala K, Laakso M. Retinopathy predicts cardiovascular mortality in type 2 diabetic men and women. *Diabetes Care*. 2007;30:292–299.

7. Kawasaki R, Tanaka S, Abe S, et al. Risk of cardiovascular diseases is increased even with mild diabetic retinopathy: the Japan Diabetes Complications Study. *Ophthalmology*. 2013; 120:574–582.

8. Early Treatment Diabetic Retinopathy Study Research Group. Grading diabetic retinopathy from stereoscopic color fundus photographs—an extension of the modified Airlie House classification. ETDRS report number 10. *Ophthalmology*. 1991;98:786–806.

9. Curtis TM, Gardiner TA, Stitt AW. Microvascular lesions of diabetic retinopathy: clues towards understanding pathogenesis? *Eye (Lond)*. 2009;23:1496–1508.

10. Joussen AM, Murata T, Tsujikawa A, Kirchhof B, Bursell SE, Adamis AP. Leukocyte-mediated endothelial cell injury and death in the diabetic retina. *Am J Pathol*. 2001;158:147–152.

11. Miyamoto K, Ogura Y, Kenmochi S, Honda Y. Role of leukocytes in diabetic microcirculatory disturbances. *Microvasc Res*. 1997;54:43–48.

12. Singh M, Shin S. Changes in erythrocyte aggregation and deformability in diabetes mellitus: a brief review. *Indian J Exp Biol*. 2009;47:7–15.

13. Cho YI, Mooney MP, Cho DJ. Hemorheological disorders in diabetes mellitus. *J Diabetes Sci Technol*. 2008;2:1130–1138.

14. Babu N, Singh M. Analysis of aggregation parameters of erythrocytes in diabetes mellitus. *Clin Hemorheol Microcirc*. 2005;32:269–277.

15. Le Devehat C, Khodabandehlou T, Vimeux M. Impaired hemorheological properties in diabetic patients with lower limb arterial ischaemia. *Clin Hemorheol Microcirc*. 2001;25: 43–48.

16. Vinik AI, Erbas T, Park TS, Nolan R, Pittenger GL. Platelet dysfunction in type 2 diabetes. *Diabetes Care*. 2001;24:1476–1485.

17. Beutelspacher SC, Serbecic N, Barash H, et al. Retinal blood flow velocity measured by retinal function imaging in retinitis pigmentosa. *Graefes Arch Clin Exp Ophthalmol*. 2011;249: 1855–1858.

18. Nicolela MT, Hnik P, Drance SM. Scanning laser Doppler flowmeter study of retinal and optic disk blood flow in glaucomatous patients. *Am J Ophthalmol*. 1996;122:775–783.

19. Demiroglu H. The importance of erythrocyte aggregation in blood rheology: considerations on the pathophysiology of thrombotic disorders. *Blood*. 1997;89:4236.

20. Roorda A, Williams DR. The arrangement of the three cone classes in the living human eye. *Nature*. 1999;397:520–522.

21. Tam J, Tiruveedhula P, Roorda A. Characterization of single-file flow through human retinal parafoveal capillaries using an adaptive optics scanning laser ophthalmoscope. *Biomed Opt Express*. 2011;2:781–793.

22. Martin JA, Roorda A. Pulsatility of parafoveal capillary leukocytes. *Exp Eye Res*. 2009;88:356–360.

23. Uji A, Hangai M, Ooto S, et al. The source of moving particles in parafoveal capillaries detected by adaptive optics scanning laser ophthalmoscopy. *Invest Ophthalmol Vis Sci*. 2012;53: 171–178.

24. Arichika S, Uji A, Hangai M, Ooto S, Yoshimura N. Noninvasive and direct monitoring of erythrocyte aggregates in human retinal microvasculature using adaptive optics scanning laser ophthalmoscopy. *Invest Ophthalmol Vis Sci*. 2013;54:4394–4402.

25. Tam J, Martin JA, Roorda A. Noninvasive visualization and analysis of parafoveal capillaries in humans. *Invest Ophthalmol Vis Sci*. 2010;51:1691–1698.

26. Chui TY, Gast TJ, Burns SA. Imaging of vascular wall fine structure in the human retina using adaptive optics scanning laser ophthalmoscopy. *Invest Ophthalmol Vis Sci*. 2013;54: 7115–7124.

27. Takayama K, Ooto S, Hangai M, et al. High-resolution imaging of the retinal nerve fiber layer in normal eyes using adaptive optics scanning laser ophthalmoscopy. *PLoS One*. 2012;7: e33158.

28. Arichika S, Uji A, Ooto S, Miyamoto K, Yoshimura N. Adaptive optics-assisted identification of preferential erythrocyte aggregate pathways in the human retinal microvasculature. *PLoS One*. 2014;9:e89679.

29. Ogura Y. In vivo evaluation of leukocyte dynamics in the retinal and choroidal circulation. *Jpn J Ophthalmol*. 2000;44: 322–323.

30. Wilkinson CP, Ferris FL III, Klein RE, et al. Proposed international clinical diabetic retinopathy and diabetic macular edema disease severity scales. *Ophthalmology*. 2003;110: 1677–1682.

31. Hirose FNK, Saito K, Numajiri Y. A compact adaptive optics scanning laser ophthalmoscope with high-efficiency wavefront correction using dual liquid crystal on silicon—spatial light modulator. In: Manns F, Söderberg P, Ho A, eds. *Proceedings of SPIE*. Vol. 7885. SPIE.Digital Library; 2011. DOI:10.1117/12.873671.

32. Lasers ANSftSUo. American National Standard for the Safe Use of Lasers. American National Standards Institute. ANSIZ136. New York, NY: American National Standards Institute; 2007.

33. Bennett AG, Rudnicka AR, Edgar DF. Improvements on Littmann's method of determining the size of retinal features by fundus photography. *Graefes Arch Clin Exp Ophthalmol*. 1994;232:361–367.

34. Tam J, Dhamdhere KP, Tiruveedhula P, et al. Disruption of the retinal parafoveal capillary network in type 2 diabetes before the onset of diabetic retinopathy. *Invest Ophthalmol Vis Sci*. 2011;52:9257–9266.

35. Nagaoka T, Sato E, Takahashi A, Yokota H, Sogawa K, Yoshida A. Impaired retinal circulation in patients with type 2 diabetes mellitus: retinal laser Doppler velocimetry study. *Invest Ophthalmol Vis Sci*. 2010;51:6729–6734.

36. Clermont AC, Bursell SE. Retinal blood flow in diabetes. *Microcirculation*. 2007;14:49–61.

37. Lorenzi M, Feke GT, Cagliero E, et al. Retinal haemodynamics in individuals with well-controlled type 1 diabetes. *Diabetologia*. 2008;51:361–364.

38. Sato Y, Chen J, Zoroofi RA, Harada N, Tamura S, Shiga T. Automatic extraction and measurement of leukocyte motion in microvessels using spatiotemporal image analysis. *IEEE Trans Biomed Eng*. 1997;44:225–236.

39. Mostany R, Chowdhury TG, Johnston DG, Portonovo SA, Carmichael ST, Portera-Cailliau C. Local hemodynamics dictate long-term dendritic plasticity in peri-infarct cortex. *J Neurosci*. 2010;30:14116–14126.

40. Nishiwaki H, Ogura Y, Kimura H, Kiryu J, Miyamoto K, Matsuda N. Visualization and quantitative analysis of leukocyte dynamics in retinal microcirculation of rats. *Invest Ophthalmol Vis Sci*. 1996;37:1341–1347.